Response to Anonymous Referee #1

We sincerely thank the reviewers' careful and constructive evaluation of our manuscript. Although the manuscript was not accepted in the previous round, we have carefully considered all the comments, conducted additional analyses, and provided further clarifications to address the raised concerns and strengthen the scientific rigor of our study. Yes, single reflectivity measurement cannot uniquely determine fog properties, especially the DSD and radius, which we had stated in the revised version. However, the fundamental premise of our approach is that accurate retrieval of Liquid Water Content (LWC) through the mass absorption method provides the physical basis for estimating fog extinction. Since LWC primarily determines the extinction capacity of fog, it serves as the key variable controlling visibility reduction. The optical depth is subsequently derived by incorporating the assumed droplet size distribution, particularly the effective droplet radius, which enables the final estimation of visibility. In the revised version, we clarify that the FM-120 measurements are used as upstream, sample-internal development evidence rather than independent validation data. Specifically, the radius parameter is estimated based on a relationship established from pseudo-targets, rather than from directly observed independent measurements. Accordingly, all diagnostics derived from the same samples are explicitly labeled as sample-internal development assessments. We have also modified the manuscript to limit the interpretation of the ten 2025 fog events to evaluating local consistency and physical plausibility of the retrieved properties, rather than independent validation of retrieval performance. The Conclusion section has been further strengthened by explicitly acknowledging the need for future evaluation using held-out events, diverse fog regimes, stricter temporal and spatial collocation strategies, and improved treatment of drizzle contamination and deviations from the assumed lognormal droplet size distribution.

General comments

1. the authors base their results on a small sample size of only 10 pre-selected cases, even though a large dataset of 5 years would be available for further analysis. It remains unclear and is not discussed how the retrieval performs in cases, when fog presence is not confirmed by independent measurements, or when clouds or precipitation occur. In both manuscript scopes (methodology validation and 'proof-of-concept'), a larger, more diverse statistical sample would need to be considered with a more thorough discussion of the limitations of the approach – in which cases does it work well, and when are there large uncertainties?

Response: We thank the reviewer for this important concern regarding sample representativeness. We agree that the ten 2025 fog events alone cannot provide a comprehensive validation dataset. Therefore, we have revised the manuscript to clearly distinguish the roles of the different datasets and to avoid overstating the validation capability of the current study.

(1) The 5-year FM-120 record (2019–2023) and the 10 spring-2025 cases serve different purposes and cannot be combined into a single validation dataset. The FM-120 in-situ observations are used exclusively for algorithm development and physical constraint establishment. Specifically, they provide DSD, spectral-regime characteristics, and moment-closure relationships to examine LWC and r_m parameterizations (Sects. 2.1, 3.1–3.3). Because the predictors, pseudo-targets, and extinction-related parameters are derived from the same FM-120 spectra, these results represent sample-internal development evidence rather than independent validation. The 10 spring-2025 cases are used only as an application demonstration and local consistency assessment, where collocated Ka-band radar and DNQ3 visibility-meter observations are simultaneously available. These cases were selected using strict criteria (DNQ3 visibility continuously below 1,000 m for at least 30 min and precipitation-free conditions) to reliably evaluate whether the retrieval properties are physically reasonable under low-visibility fog conditions. Therefore, the 5-year FM-120 dataset establishes the physical basis of the retrieval framework, while the 2025 cases provide an independent application scenario but not a statistically comprehensive validation.

(2) Conditions for physically interpretable use. This proposed retrieval framework is designed for liquid, non-precipitating fog conditions. It assumes that fog droplets satisfy the Rayleigh scattering approximation underlying the LWC retrieval and therefore, is not applicable to mixed-phase and ice-phase conditions. In addition, a single-lognormal distribution is adopted as an approximation to describe the DSD and establish the moment closure relationship. Although Sect. 3.1 shows an increased occurrence of

bimodality spectra under low-visibility conditions, the extinction-oriented parameterization developed in Sect. 3.3 reduces the sensitivity of visibility estimation to this deviation and provides a robust representation of extinction variability for partially bimodal spectra. Nevertheless, cases with strong deviations from the assumed DSD structure remain a limitation of the current method and require further investigation using larger datasets.

(3) Evidence for large-uncertainty conditions and remaining limitations. To further clarify the applicability and uncertainty of the proposed method, we added new analysis in Fig. 3a–c, which summarizes the DSD-derived spectral regime and corresponding visibility categories of the development dataset (the sample selection procedure is described in Sect. 2.1). Bimodal spectra account for 6.38% of all valid observations. The event-balanced bimodal fraction is 24.07% (95% interval 9.11–40.04%) at 100–200 m, 4.22% (1.45–7.96%) at 200–500 m, and 0.77% (0.03–1.79%) at 500–1,000 m. Only three events are available for 50–100 m category, resulting in a broad uncertainty range, and no observations are available below 50 m. Therefore, Fig.3 should be interpreted as a sample-internal assessment of spectral characteristics and method applicability analysis, rather than an independent validation of retrieval performance or a profile-level bimodality classifier. Additional analysis (Fig. 4 and corresponding reviewer response) indicates that the spectral separation between different regimes is more evident for radar reflectivity (Z), LWC, and droplet number concentration (N_T), while the separation is weaker for radius-related parameters. On the moment-closure development dataset, the optimized extinction parameterization reduces the mean absolute relative error (MARE) from 10.88% for the direct baseline approach to 9.37%; however, larger uncertainties remain under weak-reflectivity conditions ($-50 \leq Z < -35$ dBZ), where the error increases to 22.01%. These results highlight the current limitations of the method under extreme low-signal conditions. The analytical perturbation analysis is exploratory, and independent LWC observations are not available for direct validation. We have therefore revised the manuscript to clearly state that future evaluation requires larger independent datasets, stricter radar–in situ collocation, additional fog regimes, and improved treatment of non-lognormal DSDs and drizzle contamination.

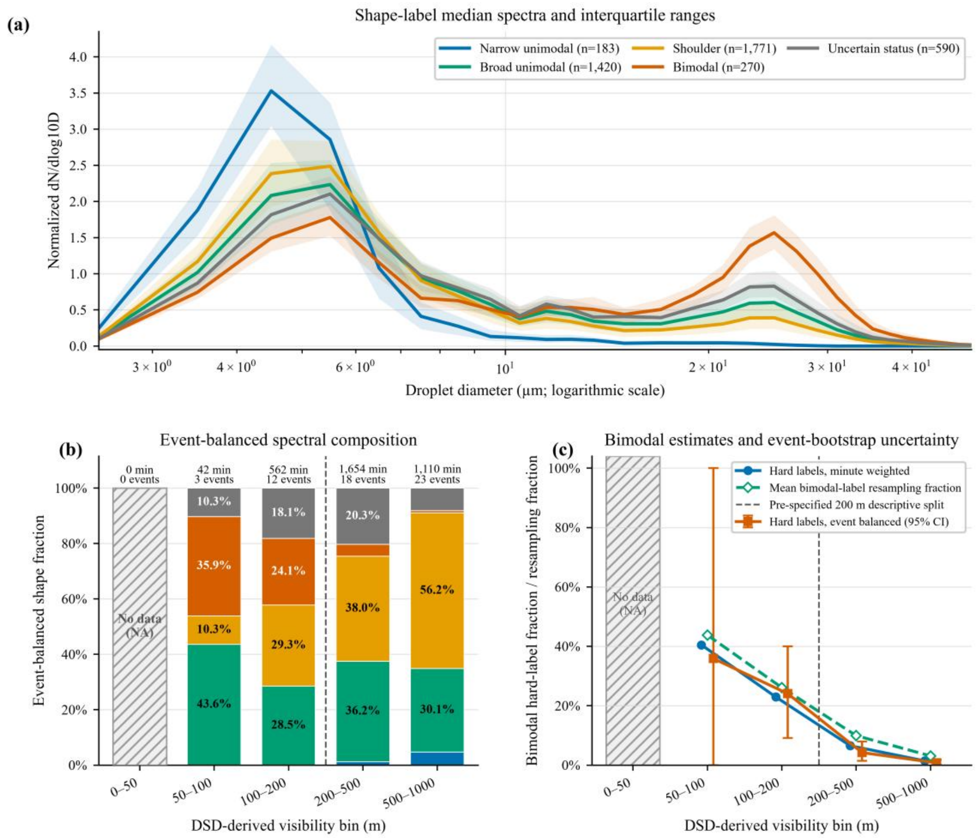

Figure R1. Revised version of Fig. 3 in the manuscript (spectral-regime characterization). Data source: FM-120 spectral-regime dataset comprising 4234 valid 1-min spectra from 28 fog events (2019–2023) at the Datan Observation Base. Method: each spectrum was classified into one of four shape categories (narrow unimodal, broad unimodal, shoulder, bimodal) or an uncertain status; event-balanced hard-label fractions were computed in DSD-derived visibility bins ([0,50), [50,100), [100,200), [200,500), [500,1000) m), with 95% intervals from 1000 complete-event resamples.

2. The authors claim that their novel method "exhibited consistent Vis variation trends" (L271) with "superior stability and smaller retrieval errors compared to the traditional empirical methods" (L294). Yet, based on results illustrated in Figs 7(e) or Fig 9(a), the correlation between observed and retrieved visibility seems very low (Fig 9), and variability does not correspond to independent vis-meter measurements (Fig 7). Reasons for mis-matches often seem speculative.

Response: We thank the reviewer for highlighting this issue and agree that the previous claims were not fully supported by the evidence presented. Accordingly, the statements about "consistent Vis variation trends" and "superior stability and smaller retrieval errors" have been removed from the revised manuscript. In the revised Section 5, we clarify the fundamental difference between radar sampling volume and the near-surface DNQ3 point measurement, and we limit the interpretation of Figs. 8–9 to case-based demonstrations.

Fig. 10 is now used to examine whether the retrieved visibility values fall within a reasonable observational range and exhibit local consistency under DNQ3-conditioned comparisons. These analyses are not presented as independent validation or quantitative ranking of retrieval methods. The comparison shows that the proposed retrieval, the site-specific FM-120-based relationship, and the empirical relationship from Liu et al. (2019, Eq. 7) produce broadly comparable visibility ranges relative to DNQ3 measurements, whereas the relationship reported by Gultepe et al. (2009, Fig. 10b) exhibits larger deviations for the selected cases. However, the available observations are insufficient to determine the underlying causes of these differences, and such differences should not be interpreted as evidence of regional or fog-regime transferability.To improve transparency, we have revised Table 1, figure legends, and captions to explicitly specify the identity, source, and application conditions of all comparison methods.

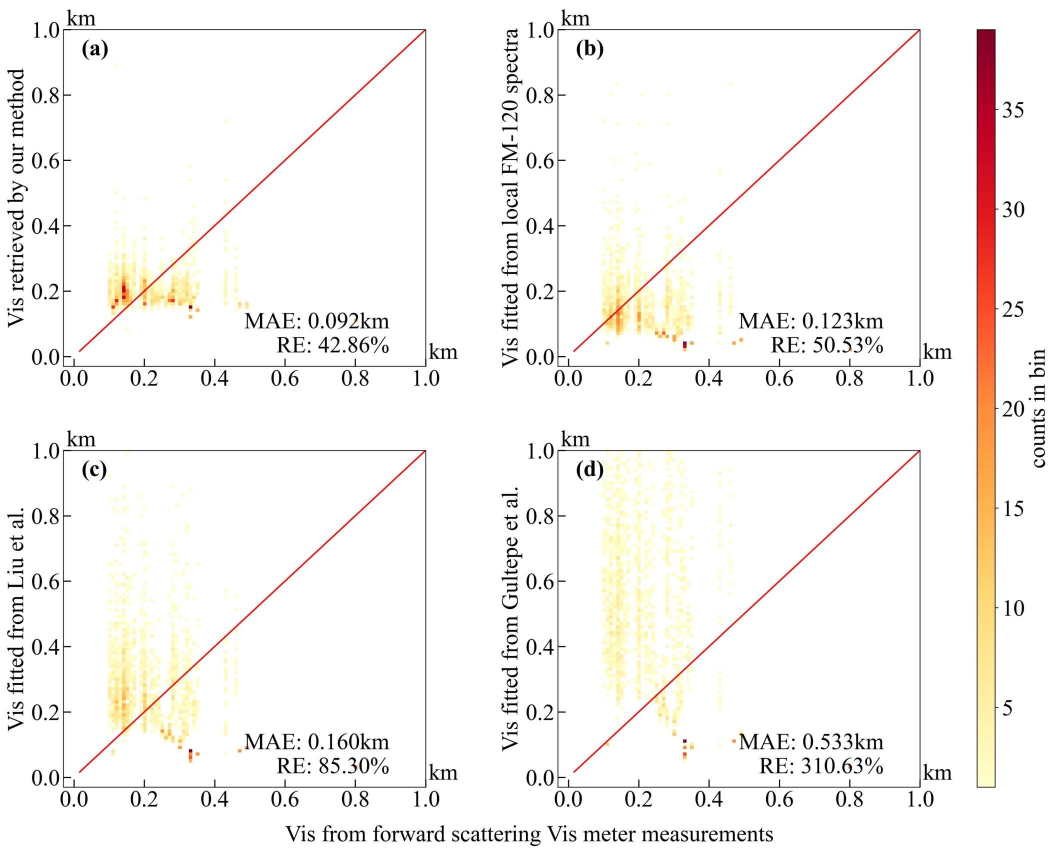

Figure R2. Revised version of Fig. 10 in the manuscript (consistency between retrieval and observation). Data source: ten criterion-selected spring 2025 fog events (DNQ3 visibility < 1000 m for at least 30 min) observed with the YLUKA2 Ka-band radar and DNQ3 forward-scatter visibility meter at the Datan Observation Base. Method: radar-derived visibility from the ~300-m range gate along the 150-degree azimuth was compared against co-located DNQ3 measurements and three empirical Vis–Z relations (the local FM-120 exponential relation, Liu et al. 2019, and Gultepe et al. 2009); axes in km with 1:1 reference lines.

3. There are a number of methodological limitations to the approach in itself which the authors mention in part:

- *Deriving LWC from single-frequency radar has high uncertainties as outlined in numerous state-of-the-art publications as the problem of retrieving two moments of the drop-size distribution with one measurement is ill-defined. The authors remain vague how much this uncertainty affects (and inhibits) the accuracy of their visibility retrieval.*

Response: We thank the reviewer for raising this important point. Indeed, conventional LWC retrieval approaches based on empirical or theoretical relationships among DSD, radar reflectivity (Z), and LWC are subject to considerable uncertainties because Z is highly sensitive to particle size distribution and therefore does not uniquely constrain liquid water content. The LWC retrieval method adopted in this study is based on the mass absorption principle, which we previously developed (Ge et al., 2023). This approach exploits the fundamental property that, under Rayleigh scattering conditions, radar attenuation is determined by the integrated liquid water mass along the propagation path rather than by the detailed droplet size distribution. The mass-absorption method adopted in this study (Ge et al., 2023) mitigates this issue fundamentally: under Rayleigh scattering, radar attenuation is proportional to the integrated liquid water mass along the propagation path, with much weaker dependence on DSD shape. Quantitatively, this method achieves a median fractional error of 37.6% for LWC retrieval, which is lower than the 45.6% error of typical reflectivity-based empirical approaches.We have further clarified the full uncertainty propagation chain in Sect. 4.2 of the revised manuscript. The analytical relative extinction response is derived as: $f = \alpha^{-\frac{4}{9}}\lambda^{\frac{32}{27}} - 1$, where α and λ are multiplicative perturbations to r_m and LWC, respectively.. A 10% increase in LWC raises extinction by 8.1%, whereas a 10% increase in r_m reduces extinction by only 4.1%. This confirms that LWC retrieval error is the dominant uncertainty source in the final visibility estimate.

- *The authors introduce numerous empirical formulas throughout the manuscript (e.g., L 183; L 268) without backing up how they were derived, or if state-of-the-art approaches were used. This should be clarified throughout the manuscript.*

Response: We thank the reviewer for pointing this out. In the revised manuscript, all empirical formulas have been explicitly documented and cross-referenced in the revised manuscript with their derivations, assumptions, and data sources clearly described and cross-referenced. The radius–reflectivity relation (formerly L 183) is now described in Sect. 3.3. This relationship is derived from the moment structure of the assumed lognormal DSD. Specifically, radar reflectivity (Z) is proportional to the sixth moment of droplet radius, while r_m represents the characteristic scale of the same distribution. Therefore, a power-law relationship between Z and r_m provides a physically motivated closure within the observed microphysical regime rather than an arbitrary empirical fitting relationship. The provenance of the three empirical Vis-Z relations introduced at L 268 is fully documented in Table 1, which we have explicitly added cross-reference in the revised text. The three empirical visibility–reflectivity (Vis–Z) relationships introduced at L268 are now fully documented in Table 1, and the revised manuscript explicitly cross-references their origins and applicable conditions. Their derivations are summarized as follows:

Local FM-120 relation: A site-specific exponential fit ($V=20.15e^{-0.07Z}$, shown in Fig. R3) derived from 732 finite pairs on 23 dates at the Datan Observation Base. This fit serves solely as a local baseline for the same coastal environment.

Equation (7) proposed by Liu et al. (2019) is obtained from a 33.44-GHz Ka-band radar and a forward-scatter visibility meter at Ningbo Beilun Port (Fujian Province) on 15 - 16 March 2015, with a reported correlation coefficient of 0.732.

Figure 10b in Gultepe et al. (2009) is derived from 1-s FRAM-L/Lunenburg data on 27 June 2006, where Z was calculated from FMD/FM-100 DSDs rather than observed directly by radar (reported RMSE 0.2367 km, correlation −0.7118).

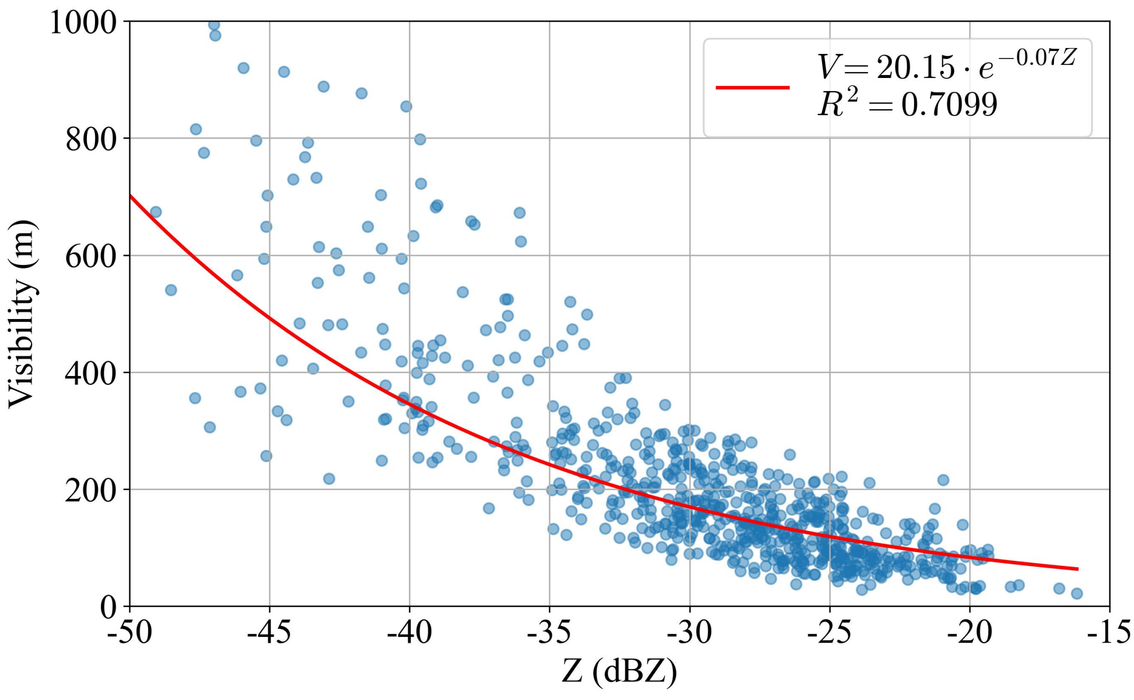

Figure R3. Local FM-120 relation. Data source: FM-120 DSD observations from 23 dates at the Datan Observation Base, yielding 732 finite Vis–Z pairs from 882 5-min aggregated records (0 < V < 2000 m).

- *DSD is assumed to be log-normally distributed (L 114). The measured DSDs could be analyzed in more detail to evaluate this assumption for the presented cases.*

Response: We thank the reviewer for this constructive suggestion. Section 3.1 and new Fig. 3a–c now analyse the spectral-regime dataset, whose sample chain is defined once in Sect. 2.1, using four hard shape labels plus an uncertain status.We have added detailed DSD shape analysis based on 5-year FM-120 observations in Sect. 3.1 and Fig. 3:

(1) Bimodal spectra account for 6.38% of all valid samples overall. The event-balanced bimodal fraction rises from 0.77% (500–1000 m visibility) to 24.07% (100–200 m visibility), indicating stronger deviation from single-lognormal assumption in dense fog.

(2) DSD shape deviation introduces structural error in the moment closure. Our extinction-oriented parameterization absorbs part of this deviation: overall extinction MAFE reduces from 10.88% (direct radius fit) to 9.37%. We explicitly state that the single-lognormal assumption is an approximation, and strong bimodality remains a limitation of the current method.

4. The metrics ("fractional error") that the authors use to evaluate the success of their retrieval is not introduced. It remains unclear how exactly this error is derived from the retrieval.

Response: We thank the reviewer for pointing out this ambiguity. We agree that the previous use of an undefined "fractional error" could lead to confusion regarding the evaluation metric and its interpretation. Therefore, this statement has been removed from the revised manuscript. For the same-source parameterization assessment, Sect. 4.1 now explicitly defines the signed fractional extinction residual as $E_\beta = (\beta_{closed} - \beta_{Mie})/\beta_{Mie}$ and MAFE as the mean absolute value of E_β.

Specific comments

1. L2: more precise information is needed on which conventional techniques the authors refer to here.

Response: Thank for pointing out this ambiguity. We now specify the conventional techniques including empirical visibility–reflectivity power-law relations (e.g., Liu et al., 2019; Gultepe et al., 2009), satellite-based retrievals, and surface forward-scatter visibility sensors in the revised Introduction part.

2. L7: also see comments above; the authors use the same radar measurement to infer LWC and visibility, thus, the information is not "independent."

Response: We thank the reviewer for pointing out this issue. The revised manuscript now clarifies that the same radar reflectivity measurement is used for both LWC retrieval and radius parameterization, and that the derived visibility should be interpreted as a conditional closure product based on the retrieved microphysical properties, rather than as an independently observed quantity. This clarification has also been incorporated into the relevant discussions to ensure that the scope and limitations of the retrieval framework are accurately represented. The word "independent" also has been removed from the Abstract and Introduction.

3. L 13: also see above; the number of analyzed cases is statistically not high enough to thoroughly validate a novel method.

Response: Thank for this comment. The revised Abstract and Conclusion clarify that the ten fog events are used only for a DNQ3-conditioned local-consistency assessment and should not be interpreted as a statistically representative validation dataset. We have also revised the conclusion to discuss the need for future evaluation using held-out events, additional fog regimes, and broader independently confirmed observations.

4. L 16: I do not think that this statement is supported by the presented analysis and high fractional error of 33.6%.

Response: Thanks for this comment. The former 33.6% fractional-error accuracy claim has been removed. The revised text presents the extinction MAFE (9.37% for the selected mapping on the moment-closure development dataset, 22.01% in the weak-reflectivity regime) strictly as same-sample development diagnostics for evaluating internal consistency of the closure relationship. We have also added appropriate caveats to clarify that these values do not represent independent validation accuracy and should not be interpreted as a direct measure of retrieval performance under broader fog conditions.

5. Line 24: a more original reference should be added here (the authors mention the classical Koschmieder Law, developed in the 1920s (Horvath, 1971) further down in the manuscript).

Response: Thanks for this suggestion. The revised text now cites Koschmieder (1924) for the visibility–extinction relation and Horvath (1971) for the subsequent application and refinement in atmospheric optics.

6. Line 36: A sentence should be added that a sensitivity to small hydrometeors is only given if Ze is not dominated by large hydrometeors in the radar volume. The authors need to discuss the additional sources of retrieval uncertainty when larger hydrometeors are present in the observed column.

Response: We thank the reviewer for this important qualification. As discussed above, the mass absorption method retrieves LWC based on radar attenuation rather than reflectivity. Because attenuation is primarily related to the integrated liquid water mass along the propagation path, this approach is substantially less sensitive to the presence of sparse large droplets that can disproportionately enhance radar reflectivity (dBZ) through their contribution to the sixth DSD moment. However, when drizzle-sized droplets (diameter >100μm) dominate the radar sampling volume, the extinction-oriented r_m–Z relation—calibrated against the FM-120 development dataset whose upper limit is 50μm —may yield a systematically biased. We have added discussion that when drizzle-sized droplets dominate the radar sampling volume, their impact on attenuation, scattering assumptions, and DSD closure requires further investigation.

7. L 54: unclear which approaches the authors refer to.

Response: We have added the relevant references for the empirical visibility–reflectivity relationships, including Liu et al. (2019, Eq. 7) and Gultepe et al. (2009, Fig. 10b), in the revised manuscript. Each relationship is now accompanied by a brief description of its data source, derivation basis, and applicable observational conditions to clarify its intended usage and limitations.

8. L 81: information on the radial scanning patterns should be added as it remains unclear whether the radar is in zenith or scan mode.

Response: Thanks for this suggestion. We have stated in Section 2 that the MMCR used plan-position-indicator (PPI) scanning at 2° elevation angle with a range-gate of 30 m.

9. L 89: variables should be introduced to the equation and units are missing.

Response: Thanks for this careful review. All variables in the blind-zone distance equation are now defined with units: 150 m × sin(2° − 0.39°/2) + 25 m, where 150 m is the minimum detection range, 2° is the radar elevation angle, 0.39° is the radar beam width, and 25 m is the antenna height.

10. L 101: The authors mention that vis-meter and cloud radar do not measure from exactly the same location. This mis-match requires a clear statement (and discussion) that the authors assume that fog microphysical properties at the surface are the same as at 30.2m height (first range).

Response: We thank the reviewer for this comment regarding spatial representativeness. In the original analysis, the first valid radar range gate along the 150° azimuth was used for comparison; however, we recognize that this choice may not provide the optimal spatial correspondence with the DNQ3 point measurement. To evaluate the sensitivity of the comparison to radar sampling distance, we examined the temporal correlation between the DNQ3 visibility record and radar-derived visibility estimates at different range gates along the 150° azimuth. The results show that the radar retrievals at approximately 300 m exhibit the strongest temporal consistency with DNQ3 measurements and were therefore selected for the revised case comparisons. Figure R2 presents the Pearson correlation coefficients between DNQ3 observations and the four visibility estimates (the proposed method, Liu et al. (2019), the local empirical relationship, and Gultepe et al. (2009)) as a function of range distance. All methods show maximum correlations within approximately 0.25–0.35 km, supporting the selection of the ~300 m range gate. We have also explicitly acknowledged that the radar retrieval represents a volumetric measurement, whereas DNQ3 provides a near-surface point observation. Therefore, despite the improved temporal correspondence at the selected range, the spatial mismatch remains an inherent limitation of the current comparison and requires further investigation using more extensive spatially collocated observations.

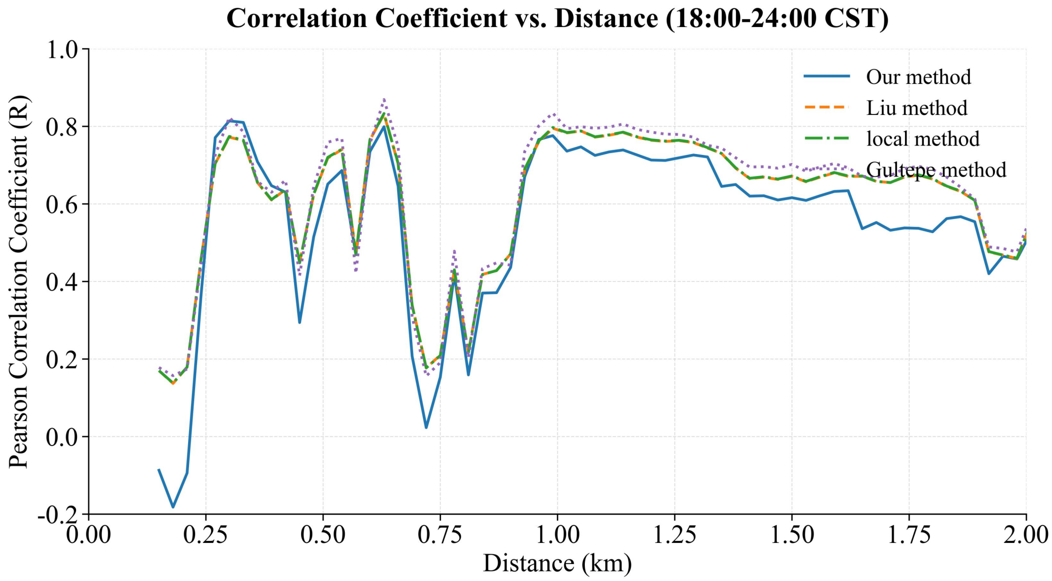

Figure R4. Correlation coefficient versus distance between the visibility meter and radar retrieval (SC10). Data source: the 2 March 2025 sea-fog case (Event 1) observed by the YLUKA2 Ka-band radar and DNQ3 visibility meter at the Datan Observation Base. Radar-derived visibility at successive range gates along the 150-degree azimuth was 5-min averaged and temporally matched with DNQ3 measurements; Pearson correlation coefficients were computed as a function of range distance for the proposed retrieval and three empirical Vis–Z relations.

11. L 138: should be Eqs 5-7.

Response: We thank the reviewer for careful review. This error has been corrected.

12. L 153: Did the authors consider correcting radar Ze for gas attenuation, and, if so, how?

Response: We thank the reviewer for raising this important question. Gas attenuation was not corrected for the Ka-band radar. Under fog conditions attenuation due to cloud liquid water is expected to dominate over gaseous absorption, while the contribution from atmospheric gases is relatively small compared with the liquid water attenuation. Therefore, gas attenuation was neglected as a first-order approximation in this study.This assumption and its potential impact have now been explicitly acknowledged in Sect. 2 of the revised manuscript. We note that although the influence of gas attenuation is expected to be minor under the targeted fog conditions, it may become relatively more important when liquid water attenuation is weak, such as in low-reflectivity cases. Future improvements will incorporate gas attenuation correction to further refine the retrieval accuracy under such conditions.

13. L 154: unclear what is meant by "microphysical coupling". Z depends on two parameters, NT and σ. If a relationship of r_m from Z alone is established, more assumptions are used than "lognormal size distribution" alone which would have to stated more clearly and discussed in more depth.

Response: We thank the reviewer for this insightful question. The term "microphysical coupling" has been replaced with more explicit and physically descriptive expressions in the revised manuscript . The radius–reflectivity relationship $r_m = aZ^b$ is motivated by the fact that both variables are related to moments of the assumed lognormal DSD, Z is proportional to the sixth moment, whereas $r_m$represents the characteristic scale parameter of the same distribution. For a lognormal DSD with a prescribed distribution width (σ), both quantities can be expressed as functions of the scale parameter, providing a physical basis for a power-law relationship between r_m and Z within the observed microphysical regime. We have now explicitly stated the associated assumptions, including a fixed DSD width (σ), single-mode lognormal DSD representation, and conditional parameterization derived from same-sample pseudo-targets, in Sect. 3.3 and discussed their implications and limitations in Sect. 4.1. We have also clarified that this relationship represents a sample-dependent closure rather than a universally applicable microphysical law. Please also refer to our detailed response to Specific Comment 16.

14. L 166: "physical transformation" is unclear.

Response: In the revised manuscript, we have clarified the mathematical formulation in Sect. 3.2. Specifically, the radar radiative transfer equation is transformed into a Bernoulli differential equation, which allows analytical integration through the cloud layer. This transformation establishes the relationship among the measured attenuated reflectivity factor (Zm), the intrinsic (attenuation-corrected) reflectivity factor (Z), and the liquid water content (LWC). The revised text now uses precise mathematical terminology and explicitly describes the role of the Bernoulli transformation in deriving the attenuation correction constraint.

15. L 176: unclear and very general; the authors should illustrate an example to outline the uncertainties originating from their LWC retrieval.

Response: We thank the reviewer for this constructive suggestion. Section 3.1 of the revised manuscript now includes an analysis of the LWC distribution (Fig. 4) based on the FM-120 spectral-regime dataset. The observed LWC characteristics are used to constrain the selection of radar profile segments, ensuring that the integrated liquid water path of each segment remains within a physically plausible range. This segmentation strategy reduces potential uncertainties associated with inappropriate initial conditions and boundary constraints during the retrieval process.

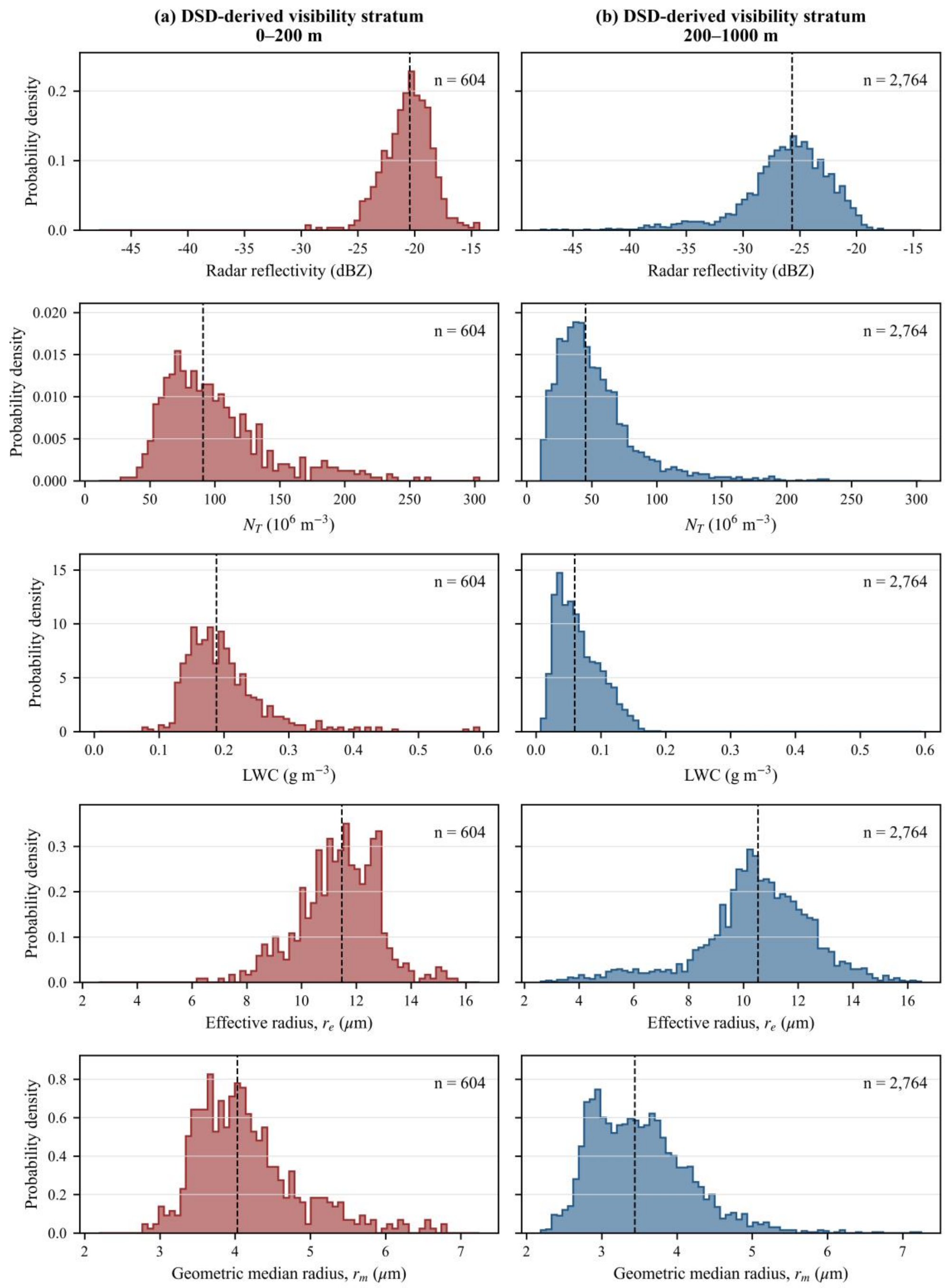

All rows use the same frozen 1-min DSD source; dashed lines are sample medians; each PDF integrates to one.

Figure R5. Revised version of Fig. 4 in the manuscript (parameter distributions). Timestamp-resolved parameter-distribution dataset derived from FM-120 DSD observations (2019–2023) at the Datan

Observation Base, comprising 188128 unique timestamps stratified by DSD-derived visibility at 0–200 m and 200–1000 m. FM-120/DSD-derived radar-equivalent reflectivity (dBZ), total number concentration (N_T), liquid water content (LWC), effective radius (r_e), and geometric median radius (r_m) were computed as discrete DSD sums at each timestamp; histograms normalized within each stratum with dashed median lines.

16. L 183: unclear why a power-law correlation is assumed, and under which conditions this empirical relation was derived – shouldn't LWC also affect this relation?

Response: We thank the reviewer for this important question. The power-law form of the $r_m - Z$ relationship is motivated by the shared dependence of both variables on the moments of the droplet size distribution (DSD). Under the assumed lognormal DSD (Eq. 4), radar reflectivity (Z) is proportional to the sixth moment of the DSD, whereas the geometric median radius (r_m) represents the characteristic scale parameter of the same distribution. Therefore, both Z and rm are controlled by the DSD scale and width (σ), providing a physical basis for a conditional power-law closure within the observed microphysical regime. We agree that LWC is also intrinsically coupled to r_m, Z, and the DSD, as it is related to the third DSD moment (Eq. 7). However, the $r_m - Z$ relationship in this study is not intended to imply that r_m is independent of LWC. Instead, it is a conditional parameterization applied after LWC retrieval and attenuation correction (Sect. 3.2). In the moment-closure development dataset, r_m pseudo-targets are obtained by minimizing extinction residuals (Eq. 13) using co-derived Z and LWC from the same FM-120 DSD observations. Thus, the fitted power law represents the sample-specific covariance between r_m and Z under the observed DSD constraints. In the retrieval sequence, LWC is first obtained through the mass-absorption method (Sect. 3.2), after which r_m is estimated from the conditional $r_m - Z$ relationship to complete the extinction calculation (Eq. 10). We have clarified this distinction in the revised manuscript to avoid any implication that r_m can be determined independently of LWC or the underlying DSD.

17. L 184: sentence should be split to facilitate readability.

Response: We thank the reviewer for this suggestion. The overly long sentence has been split into two shorter sentences for improved readability in the revised manuscript.

18. Fig 2: reference missing in the text.

Response: We thank the reviewer for catching this omission. Figure 2 (extinction efficiency Qext vs. size parameter) is now explicitly referenced in the text of Sect. 3.1, where the Rayleigh and Mie regimes are discussed in relation to the FM-120 size-bin sampling.

19. L 188: which effect will this have on the visibility retrieval? Would it lead to an over- or under-estimation of visibility in low reflectivity conditions?

Response: We thank the reviewer for this important question. The signed-residual analysis in Sect. 4.1 quantifies this behaviour. For $-50 \leq Z < -35$ dBZ, the signed mean fractional extinction residual is −21.60% for the selected mapping, indicating that the closure underestimates extinction (and therefore overestimates visibility) in this weak-reflectivity regime. The corrected result for the $-35 \leq Z < -25$ dBZ interval is a signed mean of −25.32%, confirming the same directional bias. Section 4.1 now contains the signed-residual definition, the corrected subset sizes and results, and the same-source limitation. The broader interval reports MAFE decreasing from 28.05% for the direct baseline to 22.01% for the selected mapping.

20. L 203: It is unclear if the authors interpolated the dsd from fm-120 and then did the integration of the extinction coefficient, or directly used the points of the size bins, which don't seem to sample the extinction efficiency sufficiently, as seen in Fig 4.

Response: We thank the reviewer for this clarifying question. No interpolation was applied in the calculation. For droplet radii $r>1\mu m$ (diameter $>2\mu m$), which constitute the dominant contribution to fog extinction in our observations, the oscillation amplitude of Q_{ext} is substantially damped and the bin-center value provides a close approximation to the bin-averaged Q_{ext} . For the $r<1\mu m$ region where Qext oscillations are most pronounced, the FM-120 instrument has a measurement lower limit of $2\mu m$ diameter and the radar detection capability for such small droplets is also limited. Given these instrumental constraints, interpolation in the oscillatory regime is therefore of limited significance for this study.

21. L 207: unclear – which parametrization?

Response: The parameterization here corresponds to the effective-radius and LWC relations in Eqs. (6) and (8) of the revised manuscript.

22. Fig 5: I find this 3D figure difficult to read. I suggest to instead use 2d projections of error vs r_m and error vs LWC.

Response: Thanks for this constructive suggestion. The revised manuscript now includes both the original 3D error surface and additional 2D projection panels (Fig. 6), which present the extinction residual error as a function of r_m and LWC separately. These 2D projections provide a clearer visualization of the sensitivity of the extinction residuals to each individual parameter and facilitate a more direct assessment of the parameter

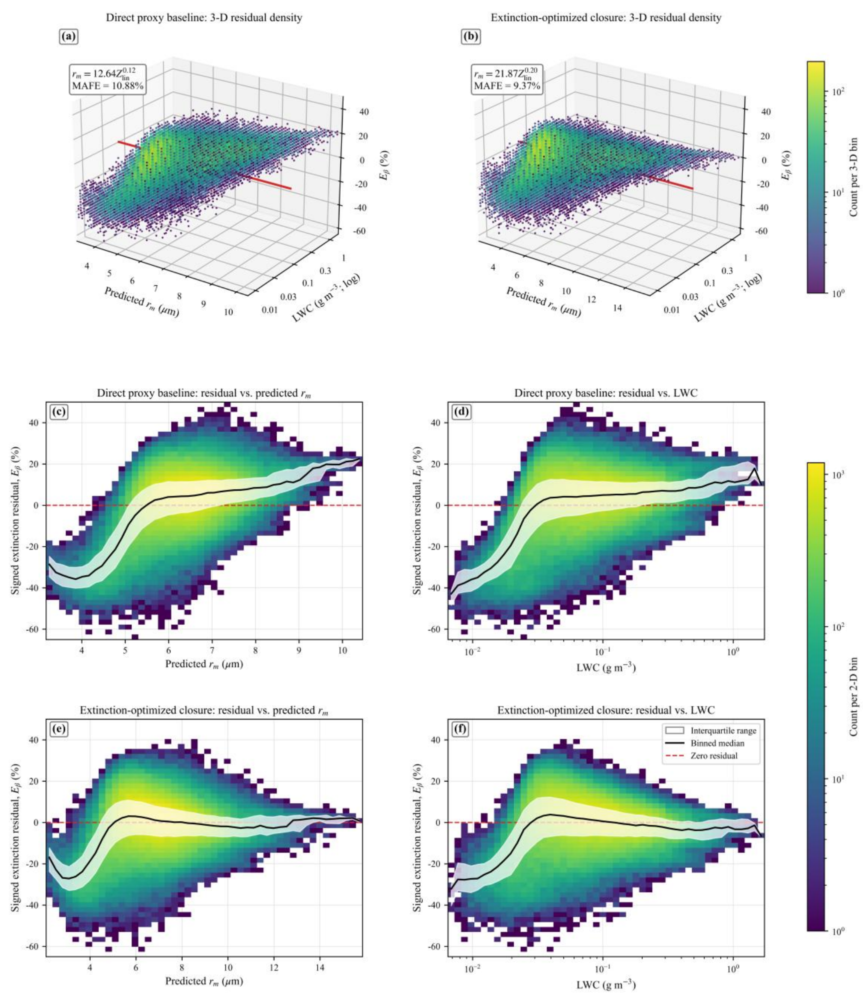

dependence of the retrieval uncertainty.

Figure R6. Revised version of Fig. 6 in the manuscript (extinction residuals). Data source: moment-closure development dataset (188214 rows) co-derived from FM-120 DSD observations at the Datan Observation Base, containing Z, LWC, r_m pseudo-targets, and Mie extinction references. Signed fractional extinction residuals $E_\beta = (\beta_{closed} - \beta_{Mie})/\beta_{Mie} \times 100\%$ were computed for both the direct r_m–Z relation and the extinction-oriented relation; 3-D residual density and 2-D projections against predicted r_m and LWC are shown with binned medians and interquartile ranges.

23. L 212: not clear which figure this refers to.

Response: We thank the reviewer for identifying this ambiguity. The sentence referred to a conceptual projection of the three-dimensional extinction residual distributions (Fig. 6) onto the LWC $-r_m$ plane, which was not explicitly presented as a separate figure in the original manuscript. To eliminate this confusion, we have removed the vague description in the revised version and now discuss the error characteristics directly in relation to the visible 3-D residual patterns shown in Fig. 6.

24. L 217: blind zone has not been introduced before, unclear what the authors refer to.

Response: The "blind zone" referred to the minimum detection range of 150 m. This potentially confusing wording has been replaced with "minimum detection range" throughout the revised manuscript.

25. L 224: Is this derived from the DSD observations?

Response: The FM-120 spectral summaries, bulk microphysical distributions, and DSD-derived visibility are all calculated from the same discrete DSD measurements. Similarly, the variables used for parameterization development are co-derived from the same FM-120 DSD samples. This same-source dependency and its implications are now explicitly stated in Sect. 3.3.

26. L 237: More information is needed on how this empirical relation is derived, and how large uncertainties are.

Response: We thank the reviewer for this important question. The revised Sect. 3.3 now provides a detailed description of the derivation and selection of the relevant parameters.

The LWC bounds are adopted from the physically plausible ranges reported in Ge et al. (2023), with a perturbation range of $0.5-2.0$. As shown in Fig. R7, the r_m range is determined based on the statistical characteristics of the present FM-120 observations, also with a perturbation range of $0.5-2.0$.

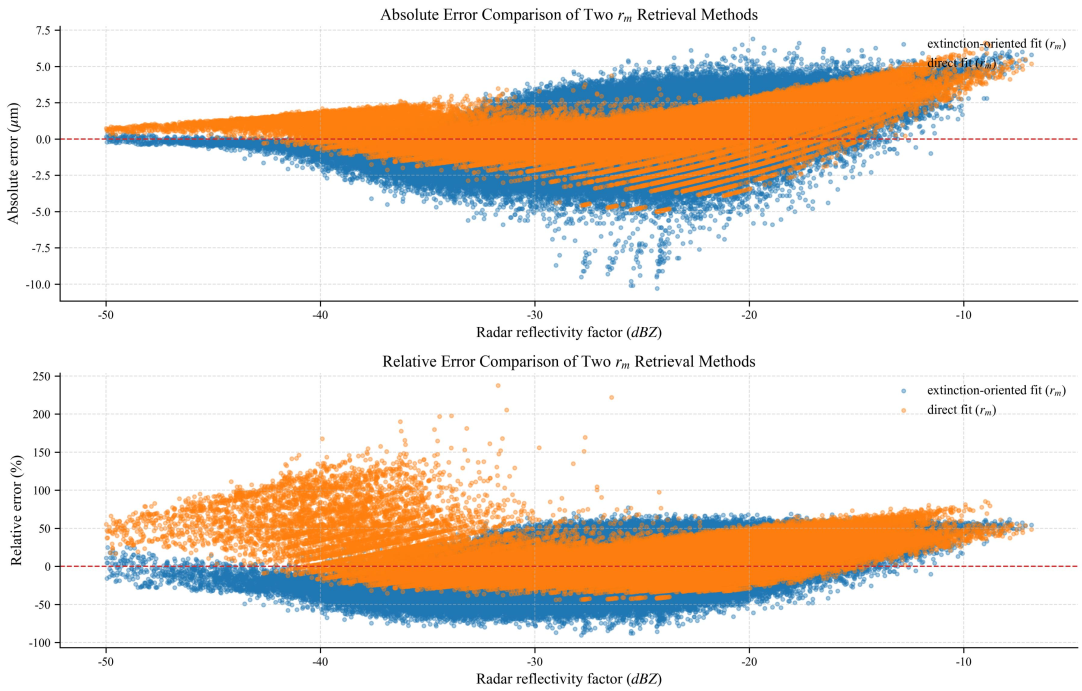

Figure R7. Comparison of absolute error (μm) and relative error (%) for extinction-oriented fit and direct fit of r_m (SC26). Data source: moment-closure development dataset co-derived from FM-120 DSD observations, using the same Z, LWC, and r_m pseudo-targets as in Fig. R8.

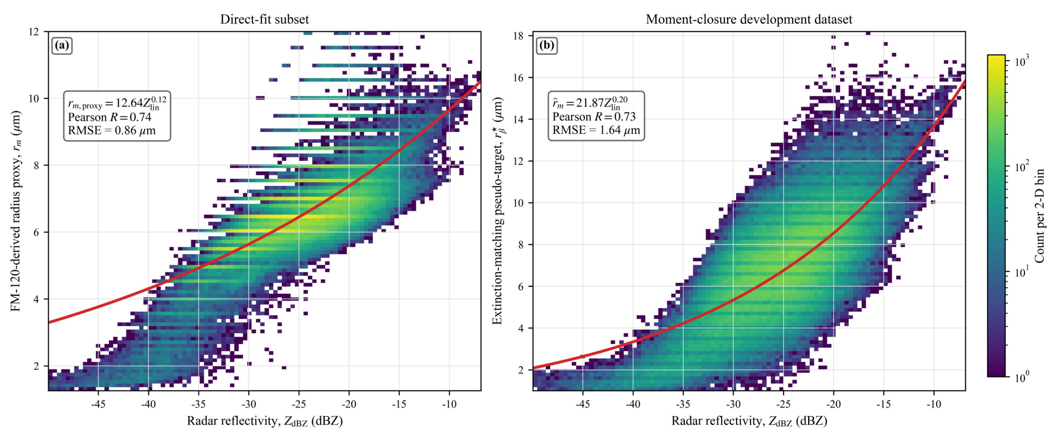

Figure R8. Revised version of Fig. 5 in the manuscript (radius relations, SC26 context). Data source: moment-closure development dataset and direct-fit subset co-derived from FM-120 DSD observations at the Datan Observation Base. For the direct fit, r_m proxy from FM-120 spectra was regressed against Z_{lin} and then fitted as $\frac{r_m}{\mu\mathrm{m}}=12.64\left(\frac{Z_{\mathrm{lin}}}{\mathrm{mm}^6/\mathrm{m}^3}\right)^{0.12}$; for the extinction-oriented fit, row-wise extinction-matching pseudo-targets were generated by minimizing extinction residuals and then fitted as $\frac{\hat{r}_m}{\mu\mathrm{m}}=21.87\left(\frac{Z_{\mathrm{lin}}}{\mathrm{mm}^6/\mathrm{m}^3}\right)^{0.20}$ by unweighted radius-space least squares; linear Z_{lin} is the predictor, dBZ is the display coordinate.

27. Fig 6: color scale should be centered around 0.

Response: Thanks for this helpful suggestion. In the revised manuscript, Fig. 7 (formerly Fig. 6) has been updated with a diverging colour map centred at zero to better highlight the symmetry of extinction residuals around the zero line.

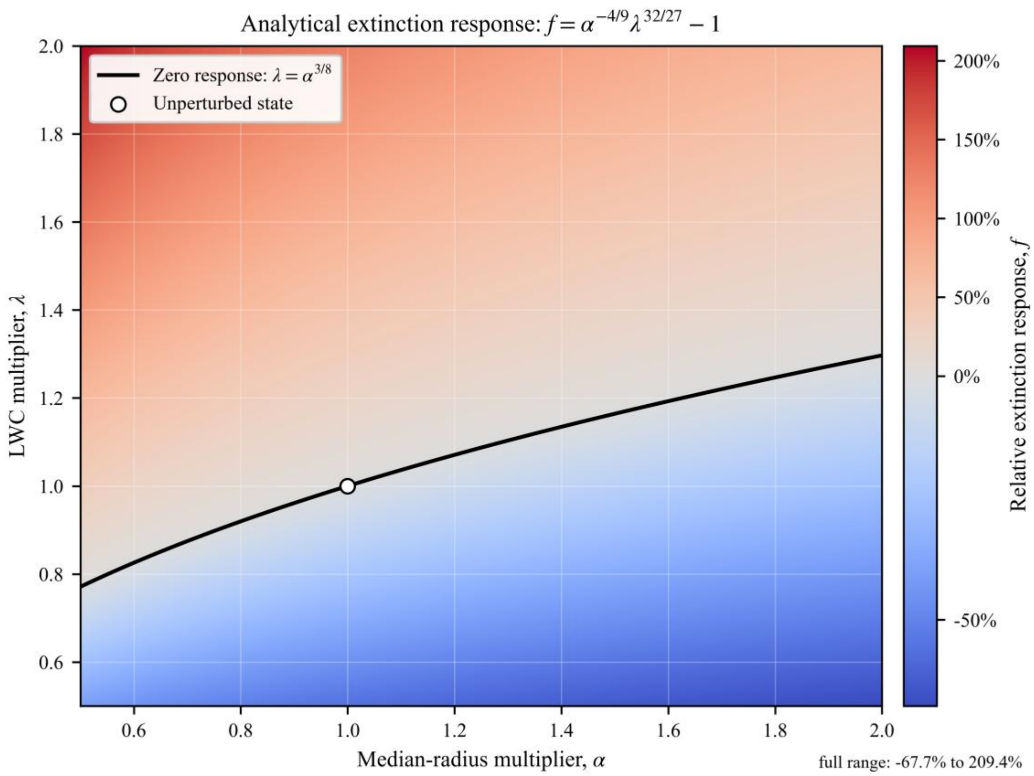

Figure R9. Revised version of Fig. 7 in the manuscript (sensitivity analysis). Data source: analytical derivation from the closed-form extinction equation (Eq. 10 in the manuscript); no external observational data used. Method: multiplicative perturbations alpha (to r_m) and lambda (to LWC) were varied from 0.50 to 2.00; the relative extinction response $f = \alpha^{-\frac{4}{9}}\lambda^{\frac{32}{27}} - 1$ was calculated on a 2-D grid, with a zero-response curve at $\lambda = \alpha^{\frac{3}{8}}$ and a zero-centred diverging colour scale.

28. L 268: unclear how this formula was derived.

Response: The derivation and provenance of the empirical formulas at L 268 are addressed in detail in our response to General Comment 3.

29. Fig 7: I find it hard to connect visibility time-series with the radar panels. Sub-panel (e) – which distance does the blue-dashed line correspond to?

Response: The case-study figure has been updated as Fig. 8, and its panel legend now explicitly identifies the DNQ3 visibility record and the four retrieval/comparison curves. Section 2 has also been revised to clarify that the radar sample used for comparison was selected from a nearby range gate (approximately 300 m along the 150° azimuth) based on its highest temporal consistency with the DNQ3 visibility variation. We acknowledge that the radar retrieval represents a volumetric measurement, whereas DNQ3 provides a near-surface point observation. Therefore, the exact gate/beam selection strategy and the sensitivity of the comparison to alternative nearby radar samples remain important limitations and are now explicitly discussed in the revised manuscript.

30. L 290: Unclear, as previously described that Fig 3 shows large deviations for small Z values.

Response: We thank the reviewer for identifying this ambiguity. The previous Fig. 3 corresponds to the weak-reflectivity diagnostic in the original manuscript is now presented in Fig. 6 in the revised manuscript. Sections 3.3 and 4.1 clarify that, within the weak-reflectivity regime ($-50 \leq Z < -35$ dBZ), the same-sample extinction MAFE is reduced from 28.05% for the direct baseline relationship to 22.01% for the selected parameterization. However, a substantial residual uncertainty remains under these low-signal conditions.

31. L 292: This statement needs to be highlighted more precisely in Sec. 4, as it is not evident to me from the presented analyses.

Response: We thank the reviewer for this suggestion for greater precision. In Sect. 4.2, the relative extinction response is derived analytically as $f = \alpha^{-\frac{4}{9}}\lambda^{\frac{32}{27}} - 1$,where α and λ are multiplicative perturbations to r_m and LWC, respectively. The ratio of the exponent magnitudes is $\frac{32}{27}\Big/\frac{4}{9}=\frac{11}{6}\approx1.83$, meaning that for any given fractional perturbation the extinction response to LWC is approximately twice that of r_m. This establishes a clear hierarchy of uncertainty sources: LWC retrieval error is the dominant contributor to final visibility uncertainty, while r_m error is secondary. We have now explicitly highlighted this priority in the opening of Sect. 4.2, emphasizing that the visibility estimate is far more sensitive to LWC perturbations than to median-radius perturbations.

32. *L 306: This is not backed up by the analysis as it was previously mentioned that temporal variability is dampened in the retrieval (L 272), and spatial variations of fog visibility were not evaluated by independent measurements.*

Response: The previous statement regarding the capability of the retrieval to capture spatial visibility variability has been removed from the revised manuscript. Section 5 and the Conclusion now clarify that the retrieval applies 4–10 range-gate averaging to reduce temporal fluctuations and improve retrieval stability, which inherently smooths small-scale variability. We further acknowledge that the spatial variability of fog visibility has not been independently evaluated in this study. Therefore, any apparent spatial structure in the retrieved visibility field should be interpreted as a consequence of the radar sampling geometry and retrieval configuration, rather than as validated evidence of the true spatial distribution of fog visibility.

References

Ge, J., et al.: A Novel Liquid Water Content Retrieval Method Based on Mass Absorption for Single-Wavelength Cloud Radar, IEEE Trans. Geosci. Remote Sens., 61, 4102815, doi:10.1109/TGRS.2023.3278735, 2023.

Gultepe, I., and Coauthors: The Fog Remote Sensing and Modeling Field Project, Bull. Amer. Meteor. Soc., 90, 341–360, doi:10.1175/2008BAMS2354.1, 2009.

Horvath, H.: On the applicability of the koschmieder visibility formula, Atmos. Environ., 5, 177–184, doi:10.1016/0004-6981(71)90081-3, 1971.

Koschmieder, H.: Theorie der horizontalen Sichtweite, Beitr. Phys. freien Atmos., 12, 33–53, 171–181, 1924.

Liu, G. P., Huang, S. Y., Liang, Y., et al.: Application of Millimeter Wave Radar in Harbor Marine Fog Observation and Visibility Inversion, J. Arid Meteorol., 37, 993–1004, doi:10.11755/j.issn.1006-7639(2019)-06-0993, 2019.

Table R1. Basic characteristics of the ten spring-2025 DNQ3-selected low-visibility cases.

Event	Period (LST)	Duration (min)	Min Vis (m)	T (°C)	Wind speed ($m\ s^{-1}$)	Wind direction (°)	RH (%)
1	2025-03-02 19:00 – 2025-03-03 05:00	600	156	19.48	3.16	219.80	97.70
2	2025-03-04 00:00 – 02:20	140	462	17.93	1.48	269.90	98.20
3	2025-03-04 05:40 – 06:10	30	563	17.67	3.32	58.10	97.20
4	2025-03-25 00:35 – 07:05	390	101	17.86	2.32	228.40	93.70
5	2025-03-26 02:20 – 08:55	395	134	18.99	3.16	219.40	90.90
6	2025-03-27 01:30 – 07:30	360	139	19.69	3.81	213.90	95.80
7	2025-03-27 20:50 – 2025-03-28 04:50	480	104	21.04	3.48	222.60	94.00
8	2025-04-10 03:25 – 08:20	295	264	20.44	1.97	235.50	96.50
9	2025-04-12 04:15 – 07:35	200	246	22.58	4.53	217.60	92.20
10	2025-04-12 11:15 – 14:40	205	455	23.93	8.05	201.90	96.40

Note: Visibility, temperature, wind speed, wind direction, and relative humidity data are from the Datan Observation Base.